on glass substrates coated with thin indium-tin-oxide (ITO) film to avoid charge-up of the sample surface during electron-beam exposure. The spin-coated films were cured by a mercury UV-lamp (intensity = 15mW/cm²) for 20min to stabilise the films. A sample with a 3.6μm thick film was chosen for the fabrication of the binary diffractive elements. Electron-beam exposure was employed to directly write a binary grating pattern with a period of d = 100μm and a 1:1 aspect ratio [7, 8]. We used a scanning electron microscope modified for electron-beam lithography, with an accelerating voltage of V = 40kV and a probe current of I_p = 10nA. Several gratings were patterned into the same film using various exposure doses. After electron beam writing, the films were post-baked at 160° for 30min to harden the films. The fabrication process is sketched in Fig. 1.

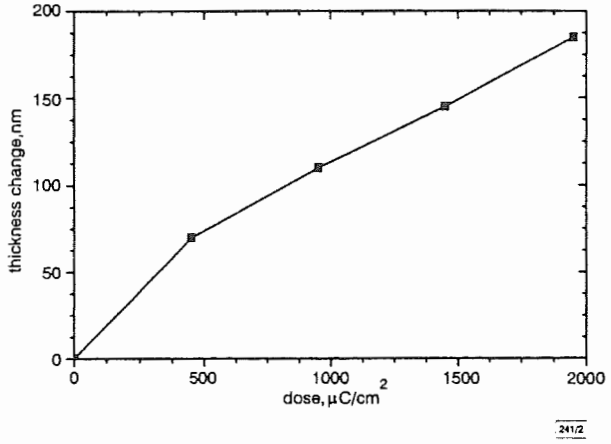

Fig. 2 *Measured decrease in film thickness against electron dose*

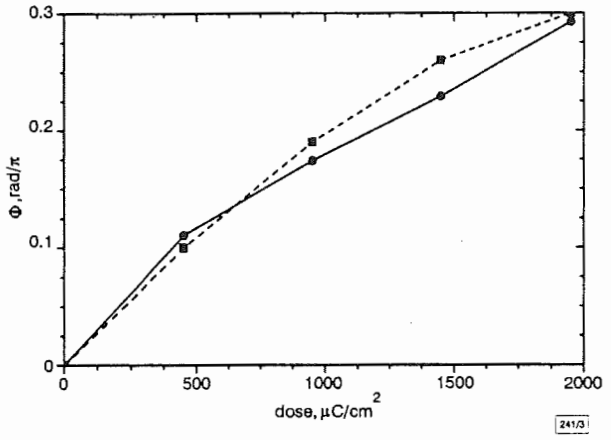

Fig. 3 *Phase delay against electron dose as determined from measured diffraction efficiencies and calculated from decrease in film thickness*

● measured
■ calculated

After the electron-beam exposure, we measured the thickness variations of the films using a surface profiler with a resolution of ~0.1nm. Fig. 2 shows the electron-beam induced decrease in film thickness as against electron dose. The phase delays were determined using an HeNe-laser (λ = 633nm), by measuring the ratio η_0/η_1 of the zeroth- and first-order diffraction efficiencies and using the complex-amplitude transmittance method. Here, $\eta_0 = |T_0|^2$ and $\eta_1 = |T_1|^2$, where T_0 and T_1 represent the zeroth and first Fourier coefficients in the expansion of the complex amplitude transmission function of the diffractive element. With the values of the coefficients known, it is straightforward to estimate the phase delays from the transmission function [7]. The resulting electron-beam induced phase delays are plotted against electron dose and shown by circles in Fig. 3. The squares in Fig. 3 depict the calculated phase delays assuming no electron-beam induced index changes, i.e. the phase delay $\Delta\phi$ is simply given as

$$\Delta\varphi = 2\pi(n_1 - n_0)d/\lambda \qquad (1)$$

in which n_1 = 1.5 (index of the sol-gel film), n_0 = 1, d is the measured etch depth, and λ is the wavelength used. The phase delays determined from the measured diffraction efficiencies and simply from the etch depth are in good agreement, suggesting that the electron-beam induced phase delays can be explained almost entirely by the decrease in film thickness. The electron-beam induced index change of the films appears to be negligible.

Conclusion: We have demonstrated direct electron-beam writing of surface relief diffractive elements into hybrid inorganic/organic sol-gel glass films. The groove depth and thus the phase delay can easily be varied by controlling the electron dose. The potential applications for this direct variable-dose 'electron-beam etching' include complex multi-phase-level diffractive elements and apodised waveguide gratings. The method combined with sol-gel waveguides seems especially attractive. The waveguides are first fabricated by UV-imprinting into hybrid sol-gel glass films and the waveguide gratings are then formed using electron-beam exposure.

The etch depths reported here are already suitable for various waveguide grating applications. In free-space diffractive elements, however, deeper structures are required to enable a full modulation range of phase delays, $0 \le \Delta\phi < 2\pi$. We believe that the full modulation range can be achieved by using successive electron-beam exposures, or by shortening the duration of UV-curing prior to electron-beam exposure.

Acknowledgments: We acknowledge the support from DARPA and the COEDIP centre and thank J.-P. Laine for his help.

5 January 1998
Electronics Letters Online no: 19980368

J.T. Rantala, N. Nordman, O. Nordman, S. Honkanen and N. Peyghambarian (*Optical Sciences Center, University of Arizona, Tucson, AZ 85721, USA*)

J. Vähäkangas (*VTT Electronics, PO Box 1102, FIN-02044 VTT, Finland*)

References

1 ANDREWS, M.P., and NAJAFI, S.I., *in* NAJAFI, S.I., and ANDREWS, M.P. (Eds.): 'Passive and active sol-gel materials and devices'. SPIE vol. CR68, Sol-Gel and Polymer Photonic Devices, 1997, pp.253–285

2 PRESBY, H.M. (Ed.): 'Silica integrated optical circuits'. SPIE Milestone Series, Vol. MS 125, 1996

3 NAJAFI, S.I. (Ed.): 'Introduction to glass integrated optics' (Artech House, Boston, 1992)

4 LI, C.-Y., CHISHAM, J., ANDREWS, M., NAJAFI, S.I., MACKENZIE, J.D., and PEYGHAMBARIAN, N.: 'Sol-gel integrated optical coupler by ultraviolet light imprinting', *Electron. Lett.*, 1995, **31**, pp. 271–272

5 SCHMIDT, H., KRUG, H., KASEMANN, R., and TIEFENSEE, F.: 'Development of optical waveguides by sol-gel techniques for laser patterning'. SPIE vol. 1590, Glass Chemistry and Physics, 1991, pp.36–43

6 ITO, T., SAKATA, M., and KOSUGE, M.: 'A novel electron beam resist system convertible into silicate glass', *IEICE Trans. Electron.*, 1993, **76**, pp. 588–593

7 NORDMAN, N., SALMINEN, O., KUITTINEN, M., and TURUNEN, J.: 'Diffractive phase elements by electron-beam exposure of thin As_2S_3 films', *J. Appl. Phys.*, 1996, **80**, pp. 3683–3686

8 NORDMAN, N., and SALMINEN, O.: 'Thickness variations in amorphous As_2S_3 films induced by electron beam', *Solid State Commun.*, 1996, **100**, pp. 241–244

Dual wavelength, 980nm-pumped, Er/Yb-codoped waveguide laser in Ti:$LiNbO_3$

J. Amin, J.A. Aust, D.L. Veasey and N.A. Sanford

The authors demonstrate the first Er/Yb codoped waveguide laser in Ti:$LiNbO_3$. The device was fabricated on x-cut $LiNbO_3$ with the guides parallel to the z-axis, resulting in reduced photorefractive damage and allowing 980nm pumping. Laser operation is demonstrated at two wavelengths, in the 1 and the 1.55μm regions, corresponding to Yb and Er transitions, respectively.

Introduction: Er:Ti:$LiNbO_3$ waveguide laser devices in $LiNbO_3$ have recently been pursued quite extensively for the realisation of devices with advanced functionality such as integrated mode-locked, Q-switched, single-frequency and tunable sources. Most devices demonstrated to date have only been pumped at 1480nm, albeit with excellent results [1]. This has mainly been due to photorefractive damage-induced instability at visible and near infrared wavelengths in this material. Recent reports on 980nm-pumped amplifier devices in Er:Ti:$LiNbO_3$ have clearly shown the detrimental effects of photorefractive damage [2]. However, given the good performance obtained using 980nm pumping in Er and Er/Yb glass devices [3], it is worthwhile investigating further techniques which will allow this pump band to be used for Er:$LiNbO_3$ devices.

To this end, we have recently utilised the z-propagation scheme for pumping devices in the near infra-red, thus allowing the first demonstration of a 980nm-pumped Er:Ti:$LiNbO_3$ laser device [4]. This propagation scheme offers high resistance to optical damage effects, as shown through the use of simple charge transport models [5]. One of the perceived disadvantages of this scheme is that it does not allow access to the high r_{33} coefficient for electro-optic modulation, but rather to the r_{22} coefficient, which is about nine times smaller. However, with proper design and optimisation of modulator structures, the half-wave voltage on z-propagating devices can be < 15V. More recently, Huang and McCaughan have also demonstrated 980nm-pumping in an Er:Zn:MgO:$LiNbO_3$ device, where Zn was used to form the waveguides in an MgO-doped $LiNbO_3$ substrate to reduce the photorefractive-induced damage [6]. The advantage of this particular device is that it allows use of the high r_{33} coefficient, but the disadvantage is that MgO-doped $LiNbO_3$ is relatively more expensive than standard $LiNbO_3$, and not of as good optical quality. Moreover, Ti has been researched more extensively than Zn for waveguide formation, and gives better yield and reproducibility, and lower loss.

In this Letter, we report our first results on Er/Yb-doped Ti:$LiNbO_3$ waveguide lasers pumped at 980nm, using the z-propagation direction, and demonstrate dual wavelength operation in these devices.

Fabrication: Alternating layers (2nm thick) of Er and Yb_2O_3 were e-beam deposited on a z-cut sample of $LiNbO_3$, to a total thickness of 28nm. The layers were then diffused into the substrate at 1100°C for a total of 360h. Ti stripes, which were 110nm thick and 7μm wide, were delineated using standard photolithography. The Ti diffusion was carried out at 1030°C for 9h. Both diffusions were carried out in flowing oxygen, in an alumina tube furnace with the sample sitting on a Pt pad. The finished devices yielded waveguides which were 2cm long.

Characterisation: The waveguides were singlemoded at 1550nm, with $1/e$ mode intensity diameters of 7.9 (±0.4) μm × 4.6 (±0.25)μm. The guides supported three transverse modes at 980 nm. Using a Ti:Al_2O_3 laser, waveguide scattering losses at the pump wavelength 980nm were estimated to be ~1.2 (± 0.1)dB.cm^{-1} (laser detuned to 910nm). Using coupled pump powers of < 2mW at 950nm, and with appropriate bandpass filters in place, the Er metastable level lifetime was measured to be 2.68 (±0.1)ms, and the Yb $^4F_{5/2}$ level lifetime was measured to be 300 (±15)μs.

The device was then CW pumped at 980nm, using end-fire techniques, with a high reflector (> 99.5% at 1530nm) butted at the input end and a 95% reflector at the output end. Both mirrors transmitted 85% of the pump light. The device lased in a stable CW mode at 1531.4nm, with a threshold of 45mW of coupled pump power, and a slope-efficiency of 0.6% (coupling efficiency ~60%). The laser characteristics are shown in Fig. 1. The absorbed pump power above threshold was measured to be 68% of the coupled pump power. The device also lased when pumped at 945nm. Given that there is minimal absorption due to Er ions at this wavelength, this is a clear indication that the lasing was not due solely to pumping of the Er ions, and that there was a transfer of energy between the Yb and Er ions.

The input and output mirrors were then replaced with mirrors which had a reflectivity of ~80% at 1060nm, for a preliminary test to see if the Yb could be made to lase at ~1μm. With the device pumped at ~945nm, stable lasing at ~1031nm was achieved at a threshold of 120mW of coupled pump power. The transmission of our mirrors at 945nm was approximately 50%. Fig. 2 shows the laser spectrum obtained using a spectrum analyser with a resolution of 0.2nm. Further characterisation of this particular laser transition in the codoped system is underway.

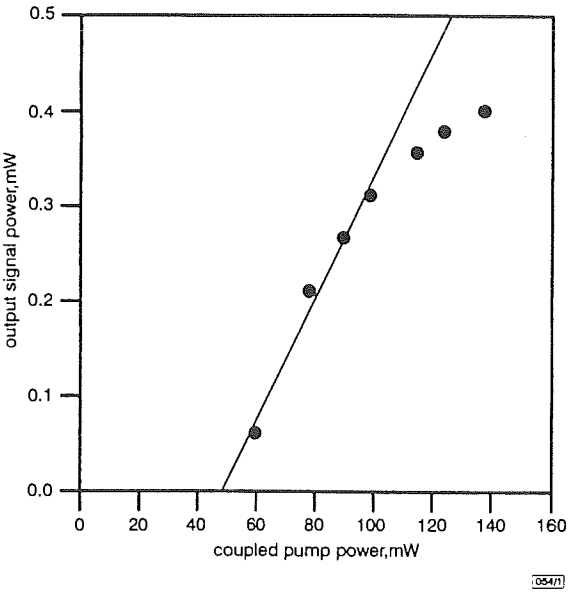

Fig. 1 *Laser characteristics for Er:Yb:Ti:$LiNbO_3$ waveguide device*
Threshold = 45mW; slope = 0.6%; λ_p = 980nm; λ_s = 1531.4nm

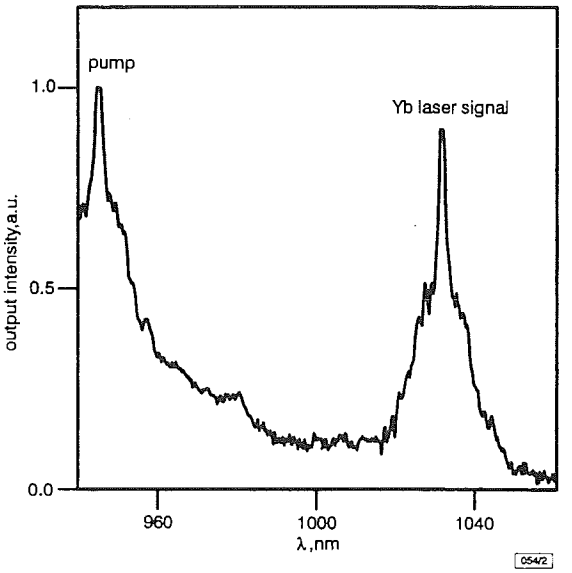

Fig. 2 *Spectrum showing Yb laser signal in codoped device*

Discussion: The measured mode sizes in this device are similar to those on our previous Er:Ti:$LiNbO_3$ device [4], indicating that the Ti diffusion conditions were not significantly different in the two samples, despite the different rare-earth diffusion conditions (144 h in the case of [4]). The relatively low output power obtained from the device is thought to be due to a combination of the high lifetime of the Er $^4I_{11/2}$ pump level (~200μs, [7]), and the finite Yb→Er transfer rate, both of which result in a 'bottlenecking' effect. This contributes to saturation of the output power at high pump powers, when the pump rate is significantly greater than the rate at which ions decay to the metastable level. This is borne out in numerical models [8]. The transfer of energy between the Yb^{3+} and Er^{3+} ions is characterised by a reduction in the Yb $^4F_{5/2}$ level lifetime. This lifetime has previously been measured to be ~600μs in Yb-diffused $LiNbO_3$ [9]. A simple rate equation analysis shows that the transfer efficiency is given by $\eta = 1 - \tau_{Yb}^{Er}/\tau_{Yb}$, where τ_{Yb}^{Er} is the Yb lifetime in the presence of Er and τ_{Yb} is the Yb lifetime without any Er. Using this equation, we estimate, to first approximation, a transfer efficiency of 50% (assuming that the Yb concentration in [9] is similar to that in our sample). The transfer

coefficients are difficult to calculate, given that the exact concentration of Er and Yb are not known in our device. However, given the low phonon energy of $LiNbO_3$ ($800cm^{-1}$), and the associated high lifetime of the Er $^4I_{11/2}$ level, backtransfer of energy from the Er to the Yb is also highly likely. The high lifetime of the pump level also results in substantial resonant ESA at 980nm from the $^4I_{11/2}$ level to the $^4F_{3/2}$ level [7]. This ESA transition results in a very strong green luminescence from the $^4S_{3/2}$ level, and may also cause a decrease in the output power due to a reduction in the population inversion. The spectroscopy of the system thus requires further investigation.

The losses in the device are higher than in our previous Er:Ti:LiNbO$_3$ [4] device, which is likely due to incomplete diffusion of the Er/Yb stack layer [10]. In the absence of known diffusion coefficients for Yb, the diffusion time for the stack layer was assumed to be similar to that required for a 28nm layer of Er at the same temperature. However, as revealed by the rough surface morphology, as seen through a microscope in the Normarski mode, the Er/Yb coupled system appears to have a substantially different diffusion coefficient. The higher losses in the device at ~1μm also mean that the laser threshold at this wavelength would be high. The device clearly needs further characterisation at this wavelength, including using mirrors which are highly reflecting at 1030nm and, perhaps more significantly, highly transmitting at 945nm.

Conclusions: We have demonstrated, for the first time to our knowledge, Er/Yb-doped Ti:LiNbO$_3$ waveguide lasers pumped at 980nm. The results obtained with these preliminary devices are very encouraging, showing that these codoped devices may be useful as multiwavelength sources. Operation in the 1 and 1.5μm regions, using a single pump, can be achieved given an appropriate mirror design which allows high reflectivity at 1030 and 1530nm, and high transmission between 945 and 980nm. These demonstration devices are, as yet, unoptimised, and it is likely that with reduced losses, better diffusion conditions, and optimisation of the Er/Yb ratios, an improved performance will be achieved.

19 December 1997
Electronics Letters Online No: 19980267

J. Amin (*SP-DV-02-5, Corning Inc., Corning, NY 14831, USA*)

E-mail: aminj@corning.com

J.A. Aust, D.L. Veasey and N.A. Sanford (*NIST, Optoelectronic Manufacturing Group, 815.04, 325 Broadway, Boulder, CO 80303, USA*)

References

1 SOHLER, W., and SUCHE, H.: 'Er-doped $LiNbO_3$ waveguide lasers', *Proc. SPIE*, 1997, **2996**, pp. 154–165

2 HUANG, C.-H., and McCAUGHAN, L.: 'Er-indiffused Ti:$LiNbO_3$ channel waveguide optical amplifiers pumped at 980nm', *Electron. Lett.*, 1996, **32**, pp. 215–217

3 SHMULOVICH, J.: 'Er-doped waveguide amplifiers on silicon', *Proc. SPIE*, 1997, **2996**, pp. 143–153

4 AMIN, J., AUST, J.A., and SANFORD, N.A.: 'Z-propagating waveguide lasers in rare-earth-doped Ti:$LiNbO_3$', *Appl. Phys. Lett.*, 1996, **69**, pp. 3785–3887

5 HOLMAN, R.L.: 'The optical properties and processing of lithium niobate optical waveguides', *Proc. SPIE*, 1983, **408**, pp. 14–20

6 HUANG, C-H., and MCCAUGHAN, L.: 'Photorefractive-damage-resistant Er-indiffused MgO:$LiNbO_3$ ZnO-waveguide amplifiers and lasers', *Electron. Lett.*, 1997, **33**, pp. 1639–1640

7 AMIN, J., DUSSARDIER, B., SCHWIEZER, T., and HEMPSTEAD, M.: 'Spectroscopic analysis of Er^{3+} transitions in $LiNbO_3$', *J. Lumin.*, 1996, **69**, pp. 17–26

8 VEASEY, D.L., GARY, J.M., AMIN, J., and AUST, J.A.: 'Time-dependent modelling of erbium-doped waveguide lasers in lithium niobate pumped at 980nm and 1480nm', *IEEE J. Quantum Electron.*, 1997, **33**, pp. 1647–1662

9 JONES, J.K., DE SANDRO, J.P., HEMPSTEAD, M., SHEPHERD, D.P., LARGE, A.C., TROPPER, A.C., and WILKINSON, J.S.: 'Channel waveguide laser at 1μm in Yb-indiffused lithium niobate', *Opt. Lett.*, 1995, **20**, pp. 1477–1479

10 BAUMANN, I., BRINKMANN, R., DINAND, M., SOHLER, W., BECKERS, L., BUCHAL, CH., FLEUSTER, M., HOLZBRECKER, H., PAULUS, H., MULLER, K.-H., GOG, TH., MATERLIK, G., WITTE, O., STOLZ, H., and VON DER OSTEN, W.: 'Erbium incorporation in $LiNbO_3$ by diffusion doping', *Appl. Phys. A*, 1997, **64**, pp. 33–44

Gain stabilisation of all-optical gain-clamped amplifier by using Faraday rotator mirrors

Y. Takushima and K. Kikuchi

The authors propose a novel configuration of all-optical gain-clamped amplifiers for suppressing the gain drift caused by polarisation fading of the feedback channel. It is shown experimentally that the gain drift of the clamped gain can be stabilised to within ±0.03dB.

Introduction: The all-optical gain clamped amplifier (GCA) is an optical amplifier which has an optical feedback path similar to that of lasers, and in which the gain is automatically clamped without any additional electrical feedback control. Previously, it has been experimentally shown that the transient response of the amplifier gain of GCAs using erbium-doped fibre amplifiers (EDFAs) can be suppressed even when the input power changes abruptly [1 – 4]. This property is attractive for the application to WDM networks where the number of wavelength channels changes dynamically.

For practical applications of GCAs, the long-term stability of the amplifier gain is another important consideration. Since the state of the laser oscillation in a GCA using an EDFA is sensitive to environmental conditions, the stability of the gain-clamping operation can easily deteriorate.

In this Letter, we discuss the gain drift induced by an interplay of polarisation-mode fluctuations and polarisation-dependent losses (PDLs), and experimentally show that the gain variation is induced in GCAs with the conventional configuration. To eliminate the gain drift, we propose a novel GCA which is composed of Faraday rotator mirrors. A Faraday rotator mirror (FRM) is a combination of a mirror and a Faraday rotator, and has been applied to remove the polarisation dependence of the device characteristics of interferometers [5], lasers [6, 7], and optical amplifiers [8]. As a new application of FRMs, we experimentally demonstrate the suppression of the gain drift due to polarisation instability.

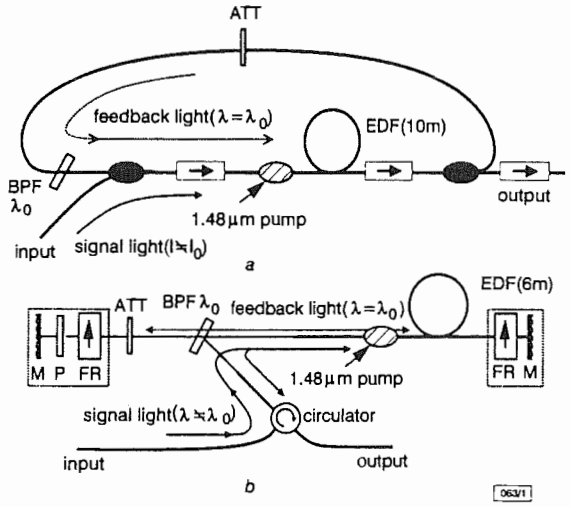

Fig. 1 *Configurations of two types of gain-clamped amplifier*

In the experiment, feedback wavelength λ_0 is set to 1561.1nm, and signal gain is measured at 1555.6nm
ATT: attenuator; EDF: erbium-doped fibre; P: polariser; M: mirror; FR: Faraday-rotator ($\pi/4$); BPF: optical bandpass filter

Gain drift induced by polarisation instability and its suppression: Fig. 1*a* and *b* show the configurations of the conventional ring-cavity GCA and the proposed GCA, respectively. They differ in their cavity configuration and stability of polarisation, but the principle of gain-clamping operation is the same. The GCA oscillates at a feedback wavelength of λ_0, and the amplifier gain is automatically set to the internal loss of the ring cavity. The signal lights are launched into the cavity, and are amplified when passing through the same gain medium. If we assume a homogenously broadened gain, the gain for the signal lights is also clamped at the internal loss for the feedback light [1].

The gain-clamping operation works well while the internal loss of the cavity is stable. However, when optical components in the